ARL-TR-10126 ● JULY 2025

On the Corrosion Behavior of Precipitation Hardenable 5XXX Series Aluminum Alloys

by Taylor W. Cain and Lindsey M. Blohm

NOTICES

Disclaimers

The findings in this report are not to be construed as an official Department of the Army position unless so designated by other authorized documents.

Citation of manufacturer's or trade names does not constitute an official endorsement or approval of the use thereof.

Destroy this report when it is no longer needed. Do not return it to the originator.

ARL-TR-10126 ● JULY 2025

On the Corrosion Behavior of Precipitation Hardenable 5XXX Series Aluminum Alloys

Taylor W. Cain and Lindsey M. Blohm
DEVCOM Army Research Laboratory

REPORT DOCUMENTATION PAGE

1. REPORT DATE	2. REPORT TYPE	3. DATES COVERED	
		START DATE	END DATE
July 2025	Technical Report	1 Sep 2022	31 Aug 2024

4. TITLE AND SUBTITLE
On the Corrosion Behavior of Precipitation Hardenable 5XXX Series Aluminum Alloys

5a. CONTRACT NUMBER	5b. GRANT NUMBER	5c. PROGRAM ELEMENT NUMBER
5d. PROJECT NUMBER	5e. TASK NUMBER	5f. WORK UNIT NUMBER

6. AUTHOR(S)
Taylor W. Cain and Lindsey M. Blohm

7. PERFORMING ORGANIZATION NAME(S) AND ADDRESS(ES)	8. PERFORMING ORGANIZATION REPORT NUMBER
DEVCOM Army Research Laboratory ATTN: FCDD-RLA-MF Aberdeen Proving Ground, MD 21005	ARL-TR-10126

9. SPONSORING/MONITORING AGENCY NAME(S) AND ADDRESS(ES)	10. SPONSOR/MONITOR'S ACRONYM(S)	11. SPONSOR/MONITOR'S REPORT NUMBER(S)

12. DISTRIBUTION/AVAILABILITY STATEMENT
DISTRIBUTION STATEMENT A. Approved for public release: distribution unlimited.

13. SUPPLEMENTARY NOTES
ORCIDs: Taylor W. Cain, 0000-0002-6621-914X; Lindsey M. Blohm, 0000-0003-1041-2511

14. ABSTRACT
The corrosion behavior of “crossover” Al-Mg-Zn-Cu–based 5XXX series aluminum was explored on nine custom alloys after several different casting and heat treatment processing routes. The results showed a strong precipitation hardening response without the need for rare or costly elemental additions. In addition, the corrosion potential and corrosion rate were shown to be sensitive to the processing route and alloy chemistry with copper showing strong effects on the electrochemical behavior while intergranular corrosion attack was not observed for all experimental alloys. Such behavior provides the opportunity to tune crossover alloys for their material properties to fit naval and non-naval applications.

15. SUBJECT TERMS
crossover alloy, 5XXX series alloy, precipitation hardenable, intergranular corrosion, Sciences of Extreme Materials

16. SECURITY CLASSIFICATION OF:			17. LIMITATION OF ABSTRACT	18. NUMBER OF PAGES
a. REPORT	b. ABSTRACT	C. THIS PAGE		
UNCLASSIFIED	UNCLASSIFIED	UNCLASSIFIED	UU	29

19a. NAME OF RESPONSIBLE PERSON	19b. PHONE NUMBER *(Include area code)*
Taylor W. Cain	(520) 691-5035

STANDARD FORM 298 (REV. 5/2020)
Prescribed by ANSI Std. Z39.18

Contents

List of Figures

List of Tables

1. Introduction

The development of advanced aluminum armor is of great importance to the U.S. Army as new materials are needed to increase agility and protection of ground vehicle systems. Aluminum-magnesium (Al-Mg)–based 5XXX series alloys remain one of the most widely used grades of aluminum alloy with 5083-H131 being the most popular. These alloys are known for their medium-strength, good ductility, good weldability, and excellent corrosion resistance, which is attractive in automotive and ground vehicle applications.[1] However, these alloys suffer from intergranular corrosion (IGC) attack due to long exposures to temperatures less than 100 °C, which can weaken the mechanical properties, worsen corrosion rates, and increase susceptibility to environmentally induced fracture.[2–4] This effect, known as sensitization, is well known and responsible for the failures of many assets, particularly in marine environments.[5] As such, new alloys need to be developed that are immune to sensitization while providing equal-or-greater material properties to currently existing alloys. A new class of Al-Mg-Zn-Cu–based 5XXX series alloys dubbed "crossover alloys" have received growing interest in open literature as they are precipitation hardenable and have been shown to resist IGC attack.[6–12]

The goal of this investigation was to determine the effect of Mg, zinc (Zn), and copper (Cu) content on the precipitation hardenability and corrosion behavior of crossover alloys. Herein, alloys were cast with a different sum of Mg + Zn + Cu with varying ratios of Mg/(Zn + Cu). The hardness versus time was measured over various temperatures to determine the peak aged (T6) heat treatment. Alloys in the solution-treated and T6 condition were then subjected to corrosion testing via potentiodynamic polarization and ASTM G67[13] nitric acid mass loss test (NAMLT).

2. Methods and Procedures

2.1 Materials

All alloys were melted and cast using an Indutherm VTC 800 V/Ti vacuum induction castings machine with 99.95 % pure pellets of Al, Mg, and Zn in addition to an Al-20Cu master alloy made in-house and commercial-grade TiCAl (Al-15Ti-0.15C) grain refiner. The charge for targeted alloy compositions (Table 1) were melted at 700 °C for 15 min and stirred every 5 min. The TiCAl grain refiner was added 10 min prior to casting and stirred into the melt. Melts were cast into an iron mold preheated to 200 °C with a rectangular cross section of 4.1 × 1.0 inches,

resulting in casting about 1450 g in mass. Two sets of alloys were made: alloys without degassing and alloys degassed by bubbling 99.999% high-purity argon in the melt for 10 min prior to casting. The alloy name designation adheres to the following conditions: the first number refers to the total sum of alloying elements (Mg, Zn, Cu) in at%; the second number is the ratio Mg/(Zn + Cu) in at%; and the third number refers to the at% Cu addition where 1 = 0.1 at% Cu, 2 = 0.2 at%, and 3 = 0.3 at% Cu. In addition, commercial alloys 5083-H131 and 5059-H131 and experimental alloy 5180-T10 were used in testing; their compositions are given in Table 2.

Table 1. Targeted composition of Al-Mg-Zn-Cu alloys used in this study.

	at%					wt%				
Alloy	**Al**	**Mg**	**Zn**	**Cu**	**Ti**	**Al**	**Mg**	**Zn**	**Cu**	**Ti**
631	Bal	4.5	1.4	0.1	0.06	Bal	3.98	3.33	0.232	0.105
632	Bal	4.5	1.3	0.2	0.06	Bal	3.99	3.10	0.463	0.105
633	Bal	4.5	1.2	0.3	0.06	Bal	3.99	2.86	0.695	0.105
641	Bal	4.8	1.1	0.1	0.06	Bal	4.27	2.63	0.233	0.105
642	Bal	4.8	1.0	0.2	0.06	Bal	4.27	2.39	0.465	0.105
731	Bal	5.25	1.65	0.1	0.06	Bal	4.64	3.92	0.231	0.104
830	Bal	6.0	2.0	0	0.06	Bal	5.28	4.74	0	0.104
831	Bal	6.0	1.9	0.1	0.06	Bal	5.28	4.5	0.230	0.104
832	Bal	6.0	1.8	0.2	0.06	Bal	5.28	4.26	0.461	0.104

Table 2. The nominal composition of commercial aluminum alloys.

Alloy	**Al**	**Mg**	**Zn**	**Cu**	**Mn**	**Zr**	**Ti**	**Fe**	**Cr**	**Ni**	**Si**
5083	Bal	4.0–4.9	0.25	0.10	0.40–1.0	. . .	0.15	0.40	0.05–0.25	. . .	0.40
5059	Bal	5.0–6.0	0.40–0.90	0.25	0.6–1.2	0.05–0.25	0.20	0.50	0.25	. . .	0.45
5180[a]	Bal	4.007	2.262	0.105	0.19	0.144	0.093	0.038	0.002	0.005	0.063

[a] The composition of 5180 was measured by inductively coupled plasma – optical emission spectroscopy.

2.2 Heat Treatments

All castings were sectioned in half vertically and one half of each casting was homogenized at 485 °C for 4 h in a muffle furnace followed by air cooling. Samples with a dimension of approximately 0.25 × 0.25 × 1.0 inch were made for further heat treatment to determine peak aging time and temperature. Samples were solution-treated at 485 °C for 1 h, water quenched, and then aged in an oil bath at either 140 or 155 °C. The hardness of samples was measured using Rockwell B hardness (HRB) while the electrical conductivity was measured as a function of percent (%) international annealed copper standard (IACS) using a Fischer Technology SigmaScope SMP10. The mean hardness and conductivity were calculated from 5 indentations and 20 conductivity measurements.

2.3 Corrosion Behavior Determination

The baseline corrosion behavior was determined using potentiodynamic polarization following modified MIL-STD-889D[14] where the open circuit potential (OCP) was monitored for 4 h and the samples were then anodically polarized from the OCP to +0.7 V above OCP unless 10 mA/cm^2 was reached first at a scan rate of 0.1 mV/s. Cathodic polarization was performed from OCP to a final potential of –1.4 V versus a saturated Ag/AgCl reference electrode at the same scan rate. All testing was performed in quiescent 3.5 wt% NaCl solution with a pH ≈ 6.25 using an electrochemical flat cell with sample working electrode, platinum mesh counter electrode, and a saturated Ag/AgCl reference electrode at room temperature. At least three repeats were performed on each measurement. Potentiodynamic polarization was also performed in some cases with a scan range of –0.3 to +0.7 V versus OCP with a scan rate of 10 mV/min. The IGC resistance of alloys was evaluated using ASTM G67[13] on samples in the T6 condition.

3. Results and Discussion

3.1 Age Hardenability

The age hardenability of the 6XY alloys is presented in Figure 1 where the hardness versus time is shown at 140 °C (Figure 1a) and 155 °C (Figure 1c) with the corresponding conductivity measurements shown in Figure 1b and 1d for 140 and 155 °C, respectively. The hardness measurements revealed the greatest peak hardness for alloys with a 3/1 ratio of Mg/(Zn + Cu) for measurements up to 256 h. At 140 °C, all 63Y alloys and alloy 641 reached a peak hardness after 128 h while alloy 642 had peak hardness after 256 h, which was the longest aging time measured in this study. For 155 °C, peak hardness was measured after 72 h for 63Y alloys and 128 h for 64Y alloys where 128 h was the longest aging time measured in this study for 155 °C. The conductivity measurements provide further insight into the aging process where increases in conductivity are present as solute is removed from the α-Al matrix to form precipitates. Theoretically, the conductivity should no longer change once the equilibrium volume fraction of the precipitates is formed and solute is no longer being removed from the matrix. For all alloys, the conductivity did not reach a plateau with the exception of alloy 632 aged 155 °C. This indicates that further aging is possible for most alloys but this does not necessarily mean that the hardness will increase with further aging time as there are likely multiple metastable phases present that contribute to the hardening response (as shown elsewhere for crossover alloys[10,15,16]).

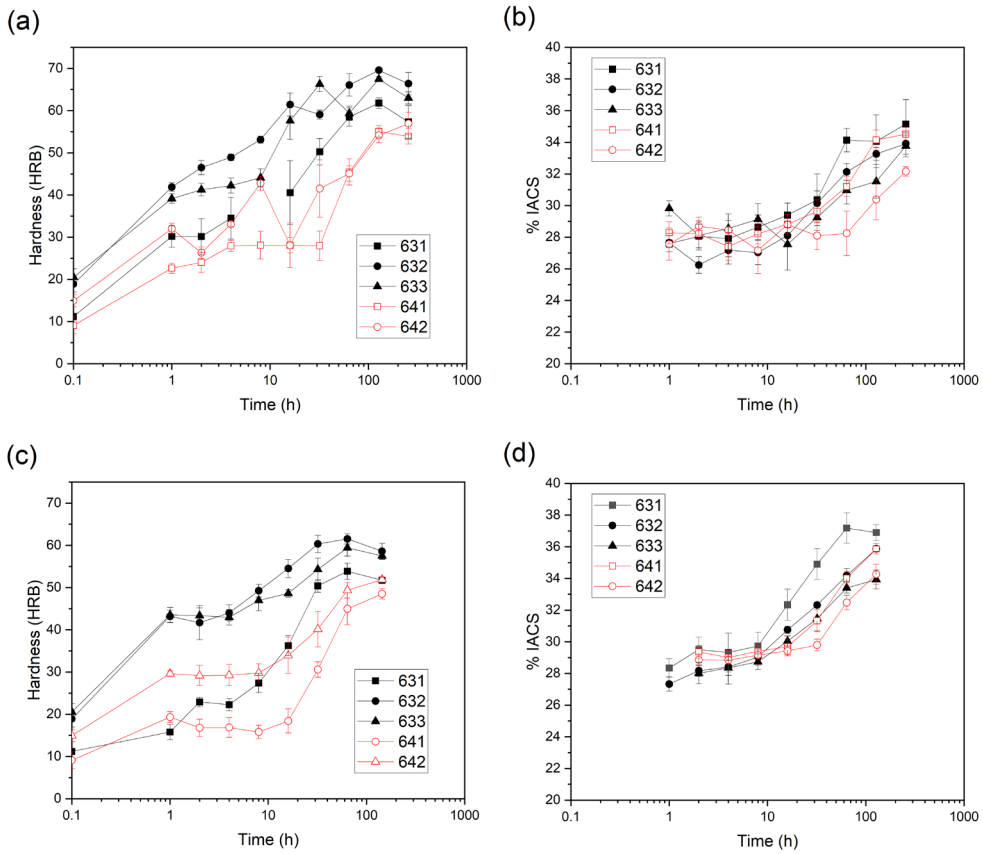

Figure 1. Age hardening plots for alloys 631, 632, 633, 641, and 642 at (a) 140 °C and (c) 155 °C with corresponding conductivity measurements (b) 140 °C and (d) 155 °C. Hardness is reported in HRB scale.

The hardness of peak aged samples with 0.1 at% Cu at 140 °C is compared to other crossover alloys made at U.S. Army Combat Capabilities Development Command Army Research Laboratory (Figure 2). This plot highlights the great age hardenability potential of crossover alloys over a range of compositions where the most rapid change in hardness is for an Mg/(Zn + Cu) at% ratio of 3. As a comparison, the hardness of 5083-H131 is typically around 53 HRB and about 69 HRB for 5059-H131. This contour plot (Figure 2) demonstrates that there is a range of compositions that can match the hardness of legacy alloys, which is promising as the hardness can be increased with additional work hardening by cold rolling or stretching. Such is the case when comparing 5180-T6 to 5180-T10 where about 20% cold work increased the hardness from about 52 to 70 HRB.

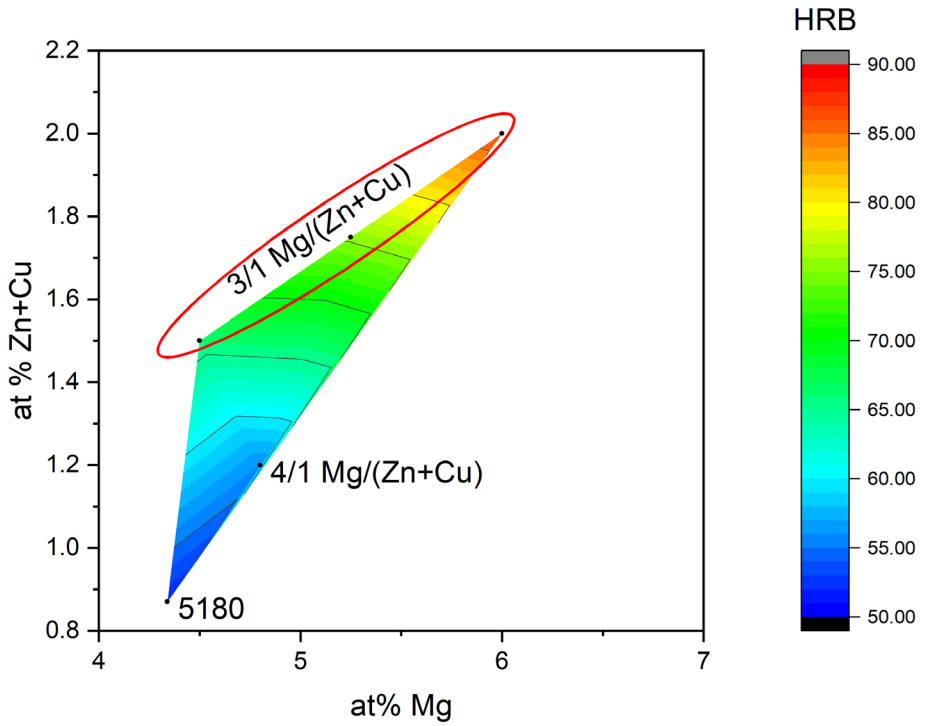

Figure 2. Contour plot of crossover alloys peak aged at 140 °C as a function of Mg concentration vs. the sum of Zn + Cu for a constant Cu concentration of 0.1 at%. Hardness is reported in HRB scale.

3.2 Polarization Behavior of Non-Degassed Castings

The baseline corrosion behavior of 6XY alloys was first assessed in the solution-treated condition. The typical OCP versus time transient, anodic polarization curves, and cathodic polarization curves are shown in Figure 3. The OCP versus time (Figure 3a) for all alloys was observed to stabilize after 2 h immersion in quiescent 3.5 wt% NaCl with a defined trend showing that increased Cu concentration led to an increase in the OCP for an equivalent Mg/(Zn + Cu) ratio. When the Cu concentration is constant but the Mg/(Zn + Cu) ratio is increased, the OCP also increased, which displays tunability of the OCP as a function of composition. For the anodic polarization of solution-treated alloys, the anodic Tafel slope (shown schematically by β_a in Figure 3b), was nearly identical for all alloys at about 25 mV/dec with no indication of passivation nor a breakdown potential. In contrast, the cathodic Tafel slope (shown schematically by β_c in Figure 3c), varied greatly from alloy to alloy (Table 3). Notably, the cathodic Tafel slope was very high (>200 mv/dec) for alloys 633, 641, and 642—indicating a large contribution of a diffusion-controlled reaction to the cathodic kinetics near OCP, which is likely to be the oxygen reduction reaction (ORR). Furthermore, the 63Y alloys exhibited a lower exchange current density for the cathodic reaction than did the 64Y alloys with alloy 632 showing the lowest cathodic exchange current density.

The corrosion potential and current density (Table 3) were performed by pairing anodic and cathodic polarization curves based on closeness in OCP and determining the intersection of the anodic and cathodic Tafel fits per MIL-STD-889D.[13] The fit parameters revealed alloy 632 to have the lowest corrosion rate of solution-treated alloys, indicating a trade-off between Cu content and corrosion kinetics. While a 643 alloy was not produced in this study, the corrosion rate for 64× alloys decreased from 641 to 642, which corroborated the trend of decreasing corrosion rate from alloy 631 to 632.

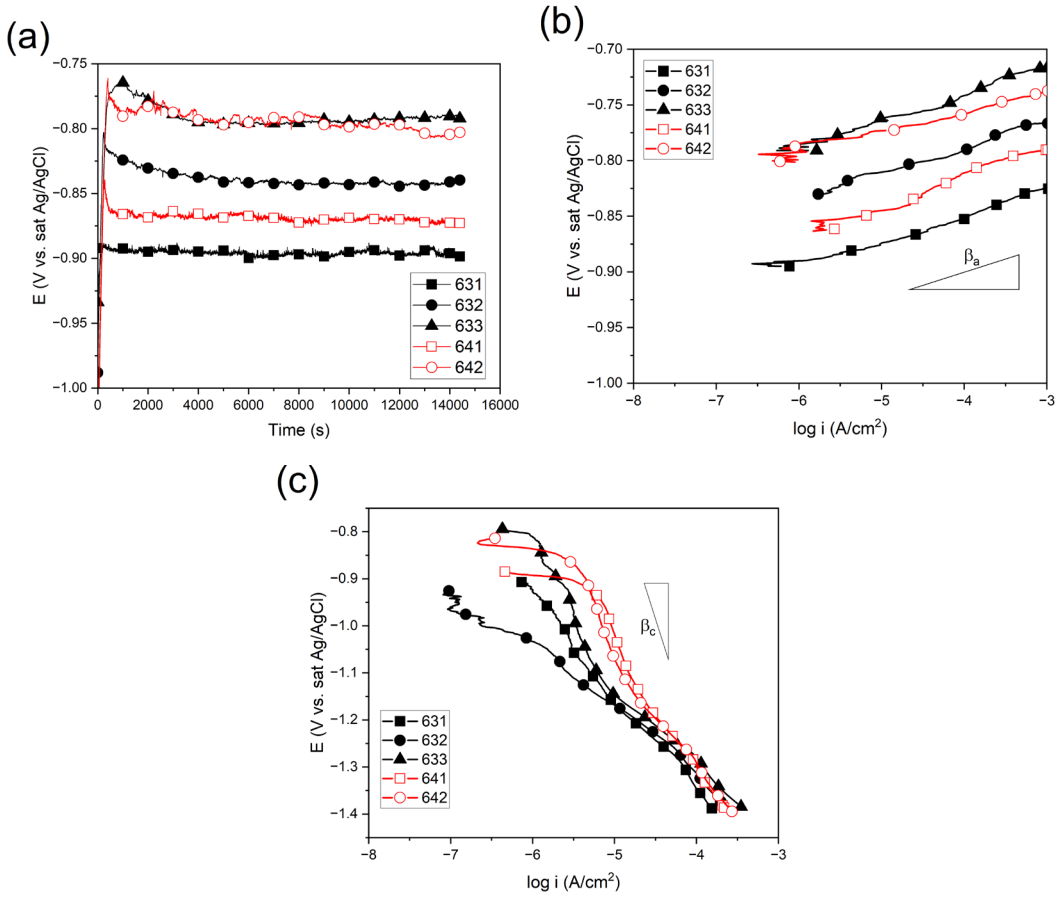

Figure 3. The typical (a) OCP vs. time for solution-treated 6XY alloys in quiescent 3.5 wt% NaCl with (b) anodic polarization and (c) cathodic polarization curves measured at 0.1-mV/s scan rate.

Table 3. Tafel fit parameters for alloys in the solution-treated condition.

Alloy	E_{corr} (V vs. sat Ag/AgCl)		i_{corr} (A/cm^2)		βa (mV/dec)		βc (mV/dec)	
	avg	std	avg	std	avg	std	avg	std
631	–0.904	6.1E-03	6.41E-07	9.3E-08	24.0	3.0	–206	5.5
632	–0.878	2.5E-03	3.87E-08	1.6E-08	26.0	1.6	–119	11
633	–0.792	1.2E-02	1.41E-06	1.8E-06	25.3	1.9	–506	118
641	–0.860	2.4E-03	2.43E-06	1.8E-06	28.3	3.4	–411	87
642	–0.793	4.2E-03	1.99E-06	4.4E-07	23.0	2.9	–494	92

In contrast to the solution-treated alloys, alloys in the peak aged condition exhibited different relative OCP and polarization behavior. Examination of the OCP transients shown in Figures 4a and 5a for alloys peak aged at 140 and 155 °C, respectively, did not display a steady OCP versus time transient like the solution-treated condition and there is no definitive trend present as a function of alloy composition. In the early stages of immersion, the OCP was observed to increase to a maximum value and then decrease, which could be indicative of native film breakdown. In many cases, the OCP experienced a sinusoidal wave behavior, which may indicate breakdown and repair of the surface film. While the OCP behavior was less stable than solution-treated alloys, the ranking of alloys at OCP was the same for 140 and 155 °C. The OCP of alloy 632 was the most negative while the OCP was similar for alloys 641, 642, and 633. Alloy 631 was the most noble of the group, which provides a great deviation in the OCP ranking in the solution-treated condition.

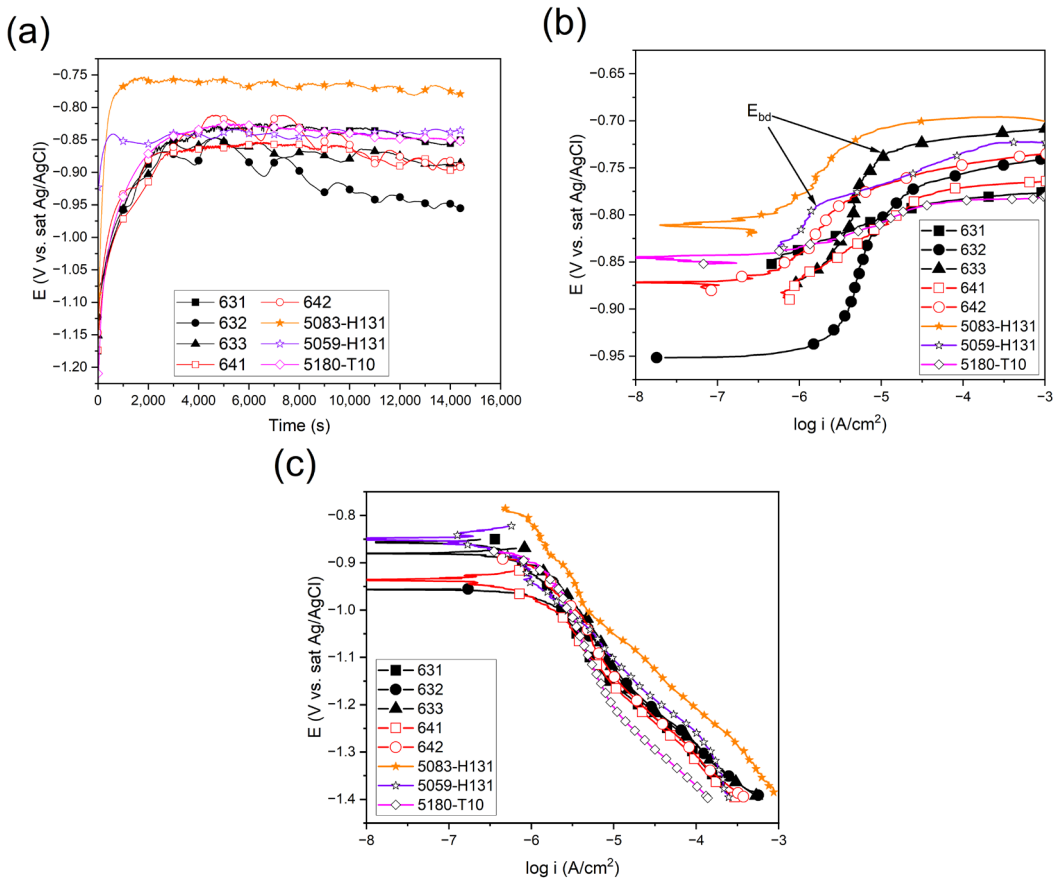

Figure 4. The typical (a) OCP vs. time for 6XY alloys peak aged at 140 °C in quiescent 3.5 wt% NaCl with (b) anodic polarization and (c) cathodic polarization curves measured at 0.1-mV/s scan rate.

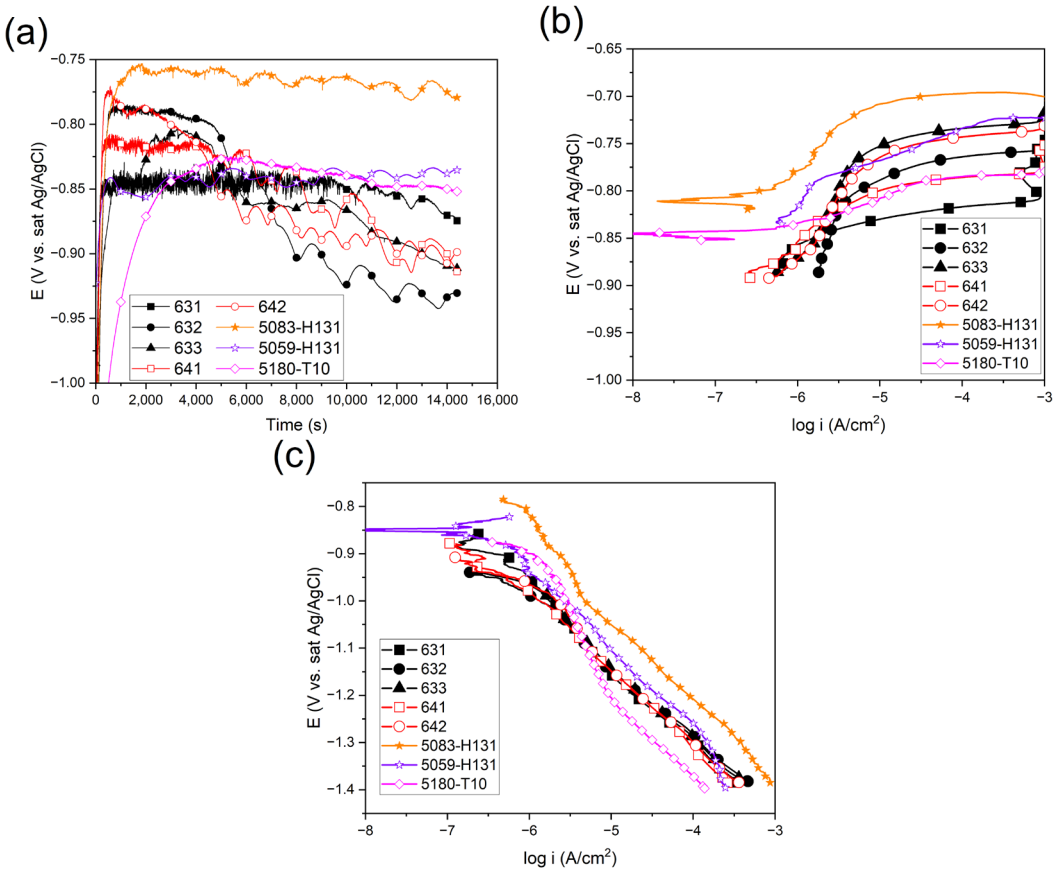

Figure 5. The typical (a) OCP vs. time for 6XY alloys peak aged at 155 °C in quiescent 3.5 wt% NaCl with (b) anodic polarization and (c) cathodic polarization curves measured at 0.1-mV/s scan rate.

The anodic polarization of peak aged alloys (Figures 4b and 5b) exhibited an increase in anodic Tafel slope compared to the solution-treated state with some cases showing a pseudo passive region of nearly vertical slope followed by a change in anodic slope whereby small increases in potential resulted in large increases in the measured current density. Examples of the breakdown potential are designated by the arrow pointing out E_{bd} in Figure 4b. The Tafel fit parameters given in Table 4 (for alloys peak aged at 140 °C) and Table 5 (for 155 °C) show that alloy 632 possessed the largest anodic Tafel slope and the largest pseudo passive window before the breakdown potential was met (i.e., $E_{corr} - E_{bd}$). The pseudo passive window was slightly larger for alloy 632 peak aged at 140 °C (254 ± 17 mV) than 155 °C (212 ± 27 mV). However, the corrosion potential was about 50 mV more anodic (i.e., more negative potential) for alloy 632 peak aged at 140 °C than it was after peak aging at 155 °C. All 63Y alloys possessed a greater anodic Tafel slope than the 64Y alloys, which indicates a greater ability for passivation. Examination of the breakdown potential provided a trend similar to the OCP and anodic polarization behavior measured on the solution-treated alloy in that increasing Cu

provided an increase in the breakdown potential for an equivalent Mg/(Zn + Cu) ratio. In addition, increasing the Mg/(Zn + Cu) ratio for an equivalent Cu concentration led to an increase in breakdown potential. One final observation on the breakdown potential is that it was more noble (i.e., more positive potential) for alloys peak aged at 140 rather than 155 °C, with the exception of alloy 642, indicating that the volume fraction of precipitates and the amount of Mg, Zn, and Cu that remain in the α-matrix can modify the breakdown potential. As the peak hardness is less at a higher aging temperature, there is likely a smaller volume fraction of precipitates present, and the equilibrium composition of the α-matrix is richer in solute at a higher aging temperature. Determination of the interplay of phase composition, volume fraction, size, and distribution is often complex and difficult to parse as the specific electrochemical behavior of sub-micrometer phases is nearly impossible to determine. When compared to 5083-H131, 5059-H131, and 5180-T10, the anodic kinetics of the 6XY are all faster (i.e., shifted to higher current density) than 5083-H131 and 5059-H131 prior to the breakdown potential while 5180-T10 behaved similarly to alloy 631 peak aged at 140 °C. Furthermore, the breakdown potential of the 6XY alloys were all more anodic than the breakdown potential of 5083-H131. However, the breakdown potential of some of the 6XY alloys were more noble than that of 5059-H131 and 5180-T10.

Table 4. Tafel fit parameters for alloy peak aged at 140 °C.

Alloy	E_{corr} (V vs. sat Ag/AgCl)		i_{corr} (A/cm^2)		β_a (mV/dec)		β_c (mV/dec)		E_{bd} (V vs. sat Ag/AgCl)		E_{corr} - E_{bd} (mV)	
	avg	std	avg	std	avg	std	avg	std	avg	std	avg	std
631	–0.853	1.0E-02	5.14E-07	1.2E-07	43.4	8.5	–225	31	–0.784	2.6E-03	69.0	13
632	–1.02	1.1E-02	2.08E-06	4.1E-07	341	44	–173	16	–0.764	7.5E-03	254	17
633	–0.907	1.1E-02	1.18E-06	2.6E-07	206	35	–218	0.89	–0.725	2.5E-03	183	12
641	–0.890	2.7E-02	6.76E-07	2.1E-07	91.3	61	–233	0.45	–0.770	1.5E-02	120	42
642	–0.863	1.6E-02	6.36E-07	1.9E-07	106	52	–209	25	–0.764	1.1E-02	98.9	26

Table 5. Tafel fit parameters for alloy peak aged at 155 °C.

Alloy	E_{corr} (V vs. sat Ag/AgCl)		i_{corr} (A/cm^2)		β_a (mV/dec)		β_c (mV/dec)		E_{bd} (V vs. sat Ag/AgCl)		E_{corr} - E_{bd} (mV)	
	avg	std	avg	std	avg	std	avg	std	avg	std	avg	std
631	–0.872	7.66E-03	4.12E-07	2.2E-07	34.9	11	–215	77	–0.826	1.2E-02	46.0	17
632	–0.984	1.95E-02	1.02E-06	3.8E-07	324	107	–152	42	–0.780	4.0E-03	204	17
633	–0.957	2.86E-02	9.30E-07	1.3E-07	267	48	–172	15	–0.745	1.9E-03	212	27
641	–0.905	2.74E-02	3.08E-07	8.4E-08	80.4	40	–151	16	–0.798	5.4E-03	107	22
642	–0.965	1.36E-02	4.83E-07	1.5E-07	176	10	–146	10	–0.756	3.3E-03	209	15

The cathodic polarization behavior of the peak aged alloys revealed little variation in the shape of the cathodic branch between alloys (Figures 4c and 5c). Two regions were observed in the cathodic branch for alloys peak aged at 140 °C with a greater Tafel slope near OCP followed by a change in cathodic slope below about –1.2 V

versus sat Ag/AgCl indicative of the hydrogen evolution reaction (HER). In general, the cathodic kinetics appeared to increase with growing Cu content, but the differences were small between different ratios of Mg/(Zn + Cu). This was also present for alloys peak aged at 155 °C where the cathodic branches lie nearly on top of each other with the primary difference being the starting potential of the scan from OCP. In comparison to 5083-H131, 5059-H131, and 5180-T10, the ORR kinetics of all 6XY alloys were slower than 5083-H131 while the ORR kinetics of 6XY alloys were similar to that of 5059-H131 and 5180-T10. The cathodic kinetics continued to follow the same trend into the HER regime except for 5180-T10, which possessed the slowest HER kinetics.

Figure 6 summarizes the corrosion potential and corrosion current density measured from polarization curves and highlights the changes in i_{corr} with alloy 632 going from the most-corrosion-resistant alloy in the solution-treated state to having one of the worst corrosion rates in the peak aged condition, which is primarily due to an increase in the exchange current density of the anodic and cathodic kinetics. Meanwhile, alloy 631 exhibited nearly constant i_{corr} regardless of the condition and increased E_{corr} in the peak aged condition, which makes it attractive for further investigation and thermomechanical processing. Furthermore, 5083-H131 possesses a low corrosion rate relative to most 6XY alloys while 5059-H131 possesses a corrosion rate in the middle of the group.

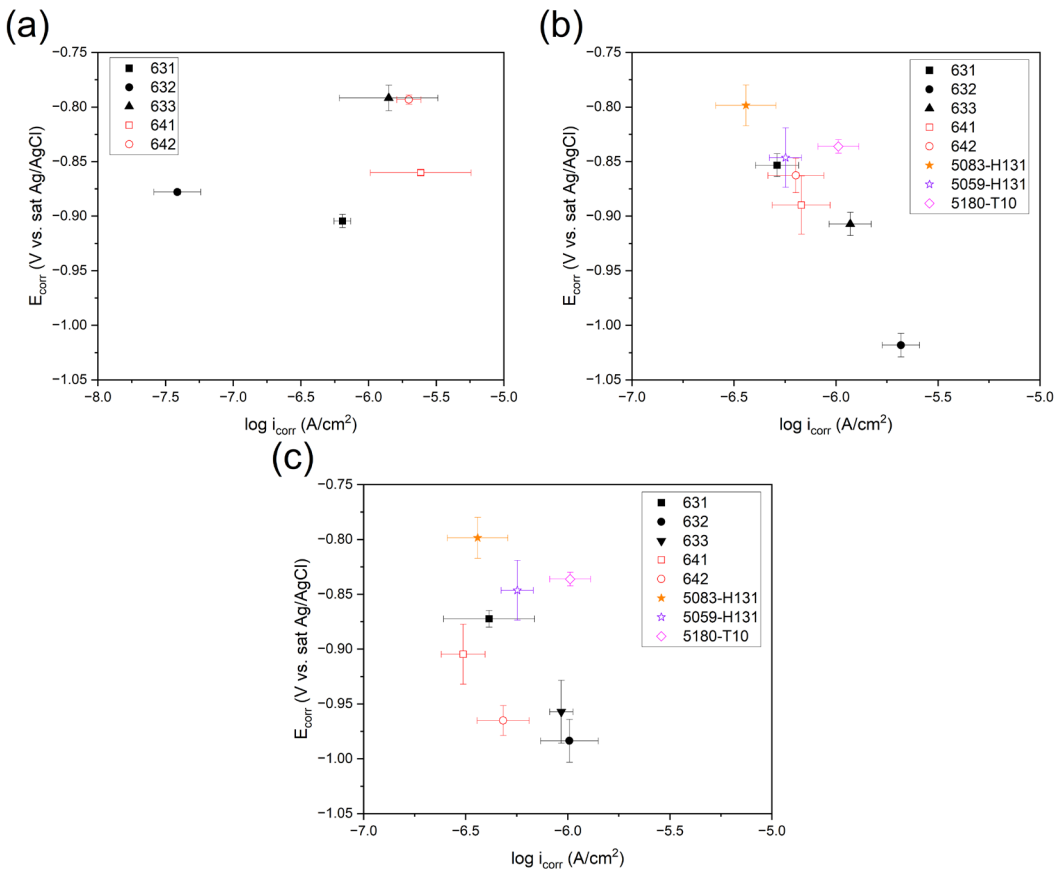

Figure 6. Plots of the corrosion potential and corrosion current density for alloys that have been (a) solution treated, (b) peak aged at 140 °C, and (c) peak aged at 155 °C. Samples were immersed in quiescent 3.5 wt% NaCl.

3.3 Polarization Behavior of Degassed Castings

Additional batches of alloys 631, 632, 641, 731, 830, 831, and 832 were produced using a degassing procedure, cast, homogenized, and heat treated to a T6 condition at 140 °C. These alloys were then tested using potentiodynamic polarization after 4 h immersion in quiescent 3.5 wt% NaCl. The typical result for each alloy is shown in Figure 7 (OCP vs. time transient is shown in Figure 7a and the potentiodynamic polarization scan is shown in Figure 7b). First, examining the OCP transients shows that 5083-H131 was the most noble alloy while alloy 830 was the least noble. From here, several interesting trends appear when comparing custom alloys to each other. When comparing the effect of total alloying element on OCP with a constant Cu concentration, the OCP was observed to follow an indirect relationship of increasing OCP with decreasing total alloy elemental concentration as shown by alloys 631, 731, and 831. In addition, the OCP was observed to increase with growing Cu concentration with a constant concentration of the total alloy element

as shown with alloy 631 versus alloy 632 and alloy 830 versus alloy 831 versus alloy 832.

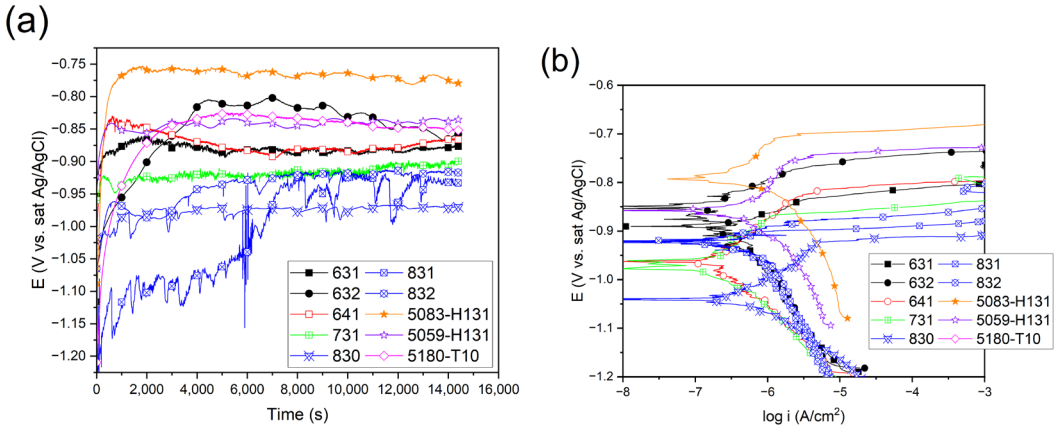

Figure 7. The typical (a) OCP vs. time and (b) potentiodynamic polarization behavior of degassed alloys 631, 632, 641, 731, 830, 831, and 832 in quiescent 3.5 wt% NaCl. Alloys were in a T6 condition after aging at 140 °C.

Examination of the potentiodynamic polarization curves in Figure 7b revealed similar trends in E_{corr} to the OCP transients as expected. In comparison to the non-degassed alloys, the degassed alloys displayed much greater variation in the anodic and cathodic kinetic behavior between alloys. Specifically, alloy 641 showed lower cathodic kinetics than alloy 631 and alloy 632 whereas the kinetic rates were very similar for non-degassed alloys shown in Figures 4c and 5c. The cathodic kinetics of alloys 831 and 832 were also similar to alloys 631 and 632 while alloy 731 displayed cathodic kinetics similar to alloy 641. Alloy 830 also showed very low cathodic kinetics but did show much more rapid anodic kinetics than the other custom alloys. Other features of the anodic kinetics include alloys 641 and 731 having similar anodic kinetics; however, alloy 641 showed a more noble breakdown potential than alloy 731. The comparison of anodic kinetics of alloys 631, 731, and 831 showed that the kinetic rate was slower with decreasing total alloy element concentration with a concomitant increase in breakdown potential with decreasing total alloy element concentration. Of the custom alloys, alloy 632 possessed the slowest anodic kinetic rate, which was bested by only 5083-H131. A plot of the mean Tafel fits for each alloy in Figure 8 summarizes much of the kinetics behavior discussed above. Alloys 641 and 731 possessed the lowest mean i_{corr} owing to the low measured anodic and cathodic reaction rates. Alloy 631 possessed a similar i_{corr} to alloys 641 and 731 but was much more noble due to its slow anodic kinetics and faster cathodic kinetic behavior. The mean i_{corr} for these three alloys was lower than that of 5083-H131 but is within error. In contrast, the 83Y alloys possessed high values of i_{corr} with alloy 830 having the fastest measured corrosion rate, which suggests that Cu is important to regulating the corrosion rate

as with the non-degassed alloys. The data in Figure 8 suggests that 0.2 at% Cu may be the optimal concentration, which deviates from the non-degassed alloys where 0.1 at% Cu was optimal. This deviation needs to be explored in further experimentation where the exact microstructural features of each alloy are characterized in greater detail than presented in this study.

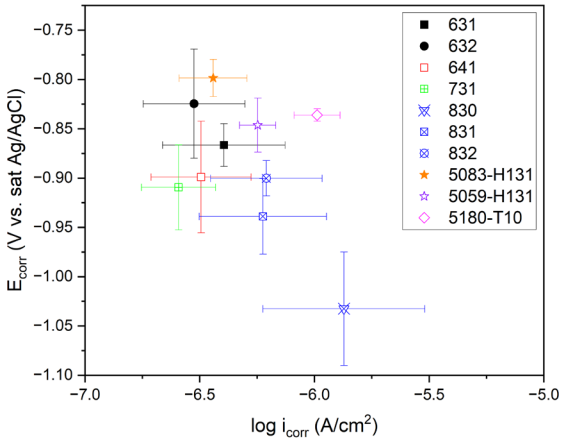

Figure 8. The mean corrosion potential and current density measured from Tafel fitting of potentiodynamic polarization tests on degassed castings.

3.4 ASTM G67 Testing

The 6XY alloys were assessed for their susceptibility to IGC on samples with peak aging at 140 °C. The results for the ASTM G67[13] NAMLT shown in Figure 9 indicated that all non-degassed alloys possessed degree of sensitization (DoS) values greater than 15 mg/cm^2, which is the threshold for alloys that are "immune" to sensitization. Furthermore, these alloys were near the 25-mg/cm^2 threshold for a sensitized alloy. Note that alloys were not subjected to a sensitization heat treatment in this study; thus, the results presented only provide a best-case scenario for resistance to sensitization. This result for non-degassed plates was surprising given results of similar crossover alloys that possessed DoS values at or below the 15-mg/cm^2 threshold. Despite these values in mass loss, each alloy did not show evidence of an IGC attack as expected with such DoS values (Figure 10). Instead, the attack appears more uniform in nature without deep penetrating IGC attack. It was theorized that impurities and cast porosity may have caused these high DoS values and select alloys were produced again incorporating an argon degassing procedure to reduce hydrogen induced porosity and remove impurities. The DoS values measured for ASTM G67 on the degassed plates were much lower than those of the non-degassed plates, which indicates success in the degassing procedure. With respect to the trends between different alloys, DoS was not observed to vary for 64Y alloys while there was some variation in the 63Y alloys. Notably, DoS was highest on alloy 632 in both conditions.

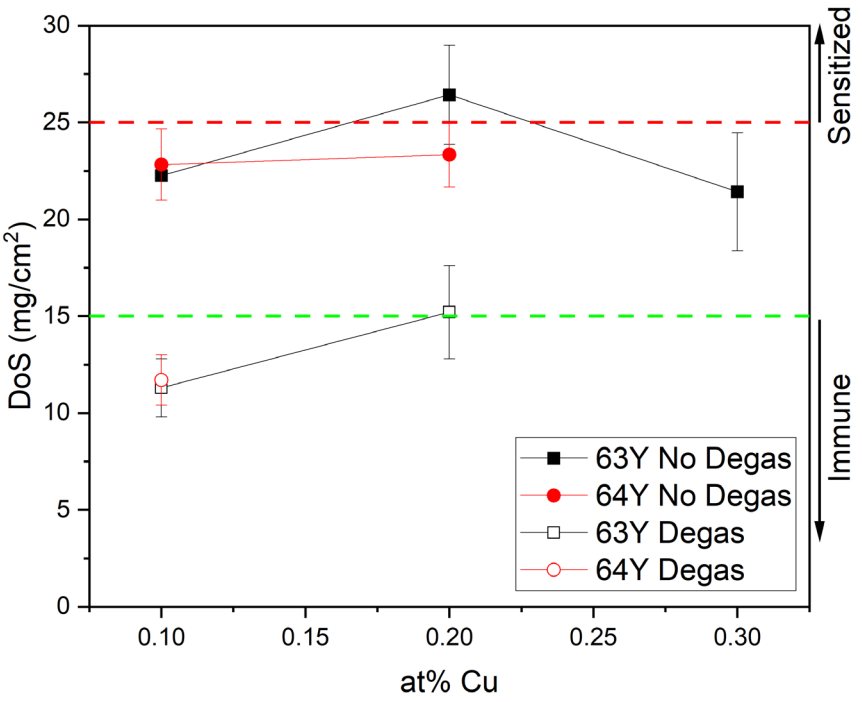

Figure 9. Plots of DoS as a function of Cu content for degassed and non-degassed castings in the peak aged condition.

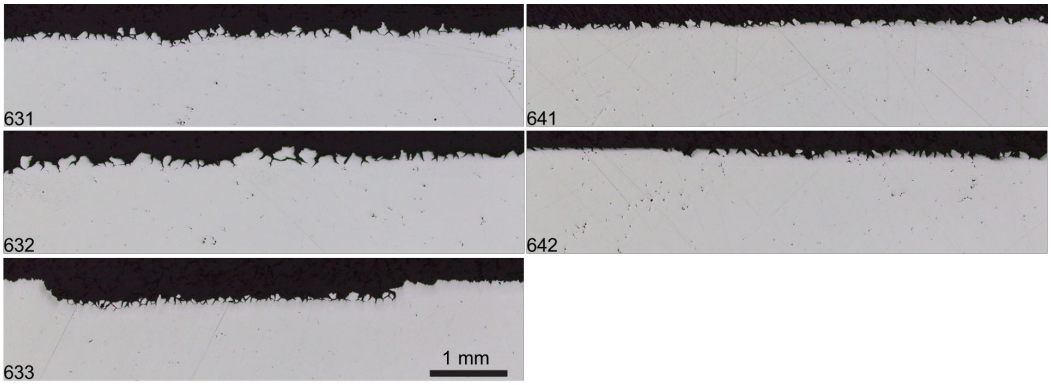

Figure 10. Optical microscopy images of non-degassed 6XY alloy cross sections after ASTM G67 testing. The 1-mm scale bar is the magnification for all images.

The DoS values of the degassed 6XY plates were compared to alloys 731, 830, 831, and 832 peak aged at 140 °C (Figure 11). The best comparison between alloys is shown for 0.1 at% Cu where DoS increases with growing total alloying content. This is likely due to the higher volume fraction of precipitates present with greater alloying content, which increases micro-galvanic activity on the alloy surface. This suggests that the total alloy content should be reduced to minimize DoS but at the sacrifice to strength. Thus, the final application for crossover alloys would need to assess the trade-off in material properties as is commonplace in materials design and selection.

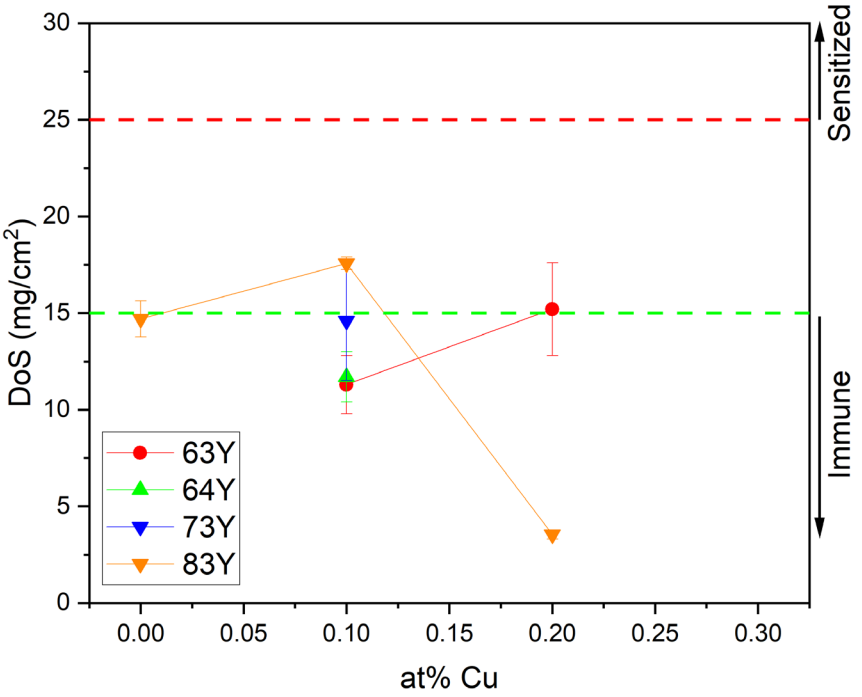

Figure 11. Plots of DoS as a function of Cu content for several degassed crossover alloy castings peak aged at 140 °C.

3.5 Brief Comments on the Potential of Crossover Alloys

This investigation briefly explored the effect of heat treatment and composition on the corrosion behavior of T-phase strengthened Al-Mg-Zn–based alloys. The results indicate that the corrosion potential and rate are controlled by the concentration of Cu and the ratio of Mg:(Zn + Cu). This provides tunability from an alloy design perspective when targeting the strength and corrosion characteristics desired for different applications. However, the alloys investigated here were from an as-cast state; structural alloys for plate application undergo thermomechanical processing via rolling and stretching, which will provide a vastly different microstructure than that present in a cast alloy. The greatest differences are expected in the grain size and texture of the resulting rolled plate, which may alter the corrosion behavior and susceptibility to different corrosion modes such as IGC, pitting, and exfoliation corrosion. To this end, further experimentation needs to be performed on rolled alloys as well as more complex alloy composition to determine the effect of other typical minor alloying elements in aluminum alloys such as Mn, Zr, Cr—as well as the impurity effects of Fe, Si, and others, common to recycling streams.

4. Conclusions

This investigation reports the hardenability and baseline corrosion characteristics of several 5XXX series crossover alloys. The following can be concluded:

- The hardenability and electrochemical behavior of crossover alloys show the ability to be tuned for a desired application. In particular, the electrochemical behavior can be tuned to be similar to legacy alloys such as 5083-H131 with equal or greater mechanical properties.
- Crossover alloys show the ability to have a pseudo passive window depending on the ratio of Mg/(Zn + Cu) and the total amount of Cu in the alloy. Further tuning of the composition and processing parameters may lead to a passive alloy.
- Crossover alloys are resistant to IGC attack and have a low DoS in the peak aged condition following ASTM 67 testing.[13]

5. References

1. Polmear IJ. Light alloys. 4th ed. Oxford: Butterworth-Heinemann; 2005.
2. Henry Holroyd NJ, Scamans GM. Environmental degradation of marine aluminum alloys—past, present, and future. Corrosion. 2015;72(2):136–143.
3. Crane CB, Gangloff RP. Stress corrosion cracking of Al-Mg alloy 5083 sensitized at low temperature. Corrosion. 2015;72(2):221–241.
4. Lim MLC, Kelly RG, Scully JR. Overview of intergranular corrosion mechanisms, phenomenological observations, and modeling of AA5083. Corrosion. 2015;72(2):198–220.
5. Golumbfskie WJ et al. Survey of detection, mitigation, and repair technologies to address problems caused by sensitization of Al-Mg alloys on navy ships. Corrosion. 2015;72(2):314–328.
6. Ma QB et al. Intergranular corrosion resistance of Zn modified 5 x x x series Al alloy during retrogression and re-aging treatment. Materials Characterization. 2018;144:264–273.
7. Ding QW et al. Strengthening mechanism of age-hardenable Al-Mg-3Zn alloys. Materials Science and Technology. 2019;35(9):1071–1080.
8. Pan YL et al. Precipitation hardening and intergranular corrosion behavior of novel Al-Mg-Zn(-Cu) alloys. Journal of Alloys and Compounds. 2021;853:157199.
9. Hou S et al. Dependence of microstructure, mechanical properties, and inter-granular corrosion behavior of Al-5.1Mg-3.0Zn-0.15Cu alloys with high temperature pre-treatment. Materials Characterization. 2020;168:110512.
10. Stemper L et al. Age-hardening response of AlMgZn alloys with Cu and Ag additions. Acta Materialia. 2020;195:541–554.
11. Stemper L et al. Giant hardening response in AlMgZn(Cu) alloys. Acta Materialia. 2021;206:116617.
12. Stemper L et al. On the potential of aluminum crossover alloys. Progress in Materials Science. 2022;124:100873.
13. ASTM G67-18. Standard test method for determining the susceptibility to intergranular corrosion of 5XXX series aluminum alloys by mass loss after exposure to nitric acid (NAMLT Test). 2018, ASTM International: West Conshohocken, PA.

14. MIL-STD-889D. Galvanic compatibility of electrically conductive materials. Army Research Laboratory (US); 2021 July 21.

15. Hou SL et al. Solute clustering and precipitation of Al-5.1Mg-0.15Cu-xZn alloy. Materials Science and Engineering a-Structural Materials Properties Microstructure and Processing. 2019;759:465–478.

16. Hou S et al. Precipitation hardening behavior and microstructure evolution of Al–5.1 Mg–0.15Cu alloy with 3.0Zn (wt%) addition. Journal of Materials Science. 2017;53(5):3846–3861.

List of Symbols, Abbreviations, and Acronyms

Ag	silver
AgCl	silver chloride
Al	aluminum
at%	atomic-percent
β	Tafel slope
Bal	balance
Cr	chromium
Cu	copper
DoS	degree of sensitization
E_{corr}	corrosion potential
Fe	iron
HER	hydrogen evolution reaction
HRB	Rockwell B hardness (scale)
IACS	international annealed copper standard
i_{corr}	corrosion current density
IGC	intergranular corrosion
Mg	magnesium
Mn	manganese
NaCl	sodium chloride
NAMLT	nitric acid mass loss test
OCP	open circuit potential
ORR	oxygen reduction reaction
Sat	saturated
Si	silicon
Ti	titanium

wt%	weight-percent
Zn	zinc
Zr	zirconium

1 (PDF)	DEFENSE TECHNICAL INFORMATION CTR DTIC OCA
1 (PDF)	DEVCOM ARL FCDD RLB CI TECH LIB